Thermosensitive polymer-grafted iron oxide nanoparticles studied by in situ dynamic light backscattering under magnetic hyperthermia

Gauvin Hemery, Elisabeth Garanger, Sébastien Lecommandoux, Andrew Wong, Elizabeth Gillies, Boris Pedrono, Thomas Bayle, David Jacob, Olivier Sandre

This document is the Accepted Manuscript version of a Published Work that appeared in final form in *J. Phys.* D: *Appl. Phys.* 48 (2015) 494001 © Institute of Physics (UK) after peer review and technical editing by IOP Publishing. To access the final edited and published work see http://dx.doi.org/10.1088/0022-3727/48/49/494001

Thermosensitive polymer-grafted iron oxide nanoparticles studied by *in situ* dynamic light backscattering under magnetic hyperthermia

Gauvin Hemery[1,2], Elisabeth Garanger[1,2], Sébastien Lecommandoux[1,2], Andrew D. Wong[3], Elizabeth R. Gillies[3], Boris Pedrono[4], Thomas Bayle[4], David Jacob[4], and Olivier Sandre[1,2*]

1 Univ. Bordeaux, LCPO, UMR5629, Bordeaux INP, 16 avenue Pey Berland 33607 Pessac, France
2 CNRS, Laboratoire de Chimie des Polymères Organiques, UMR 5629, 33607, Pessac, France
3 Department of Chemistry and Chemical and Biochemical Engineering, University of Western Ontario, London, Canada
4 Cordouan Technologies, Cité de la photonique, 11 avenue de Canteranne, 33600 Pessac, France

* olivier.sandre@enscbp.fr

Abstract

Thermometry at the nanoscale is an emerging area fostered by intensive research on nanoparticles (NPs) that are capable of converting electromagnetic waves into heat. Recent results suggest that stationary gradients can be maintained between the surface of NPs and the bulk solvent, a phenomenon sometimes referred to as "cold hyperthermia". However, the measurement of such highly localized temperatures is particularly challenging. We describe here a new approach to probing the temperature at the surface of iron oxide NPs and enhancing the understanding of this phenomenon. This approach involves the grafting of thermosensitive polymer chains to the NP surface followed by the measurement of macroscopic properties of the resulting NP suspension and comparison to a calibration curve built up by macroscopic heating. Superparamagnetic iron oxide NPs were prepared by the coprecipitation of ferrous and ferric salts and functionalized with amines, then azides using a sol-gel route followed by a dehydrative coupling reaction. Thermosensitive poly[2-(dimethylamino)ethyl methacrylate] (PDMAEMA) with an alkyne end-group was synthesized by controlled radical polymerization and was grafted using a copper assisted azide-alkyne cycloaddition reaction. Measurement of the colloidal properties by dynamic light scattering (DLS) indicated that the thermosensitive NPs exhibited changes in their Zeta potential and hydrodynamic diameter as a function of pH and temperature due to the grafted PDMAEMA chains. These changes were accompanied by changes in the relaxivities of the NPs, suggesting application as thermosensitive contrast agents for magnetic resonance imaging (MRI). In addition, a new fibre-based backscattering setup enabled positioning of the DLS remote-head as close as possible to the coil of a magnetic heating inductor to afford *in situ* probing of the backscattered light intensity, hydrodynamic diameter, and temperature. This approach provides a promising platform for estimating the response of magnetic NPs to application of a radiofrequency magnetic field or for understanding the behaviour of other thermogenic NPs.

1. Introduction

Currently, magnetic nanoparticles (NPs) stand at the forefront of research in nanomedicine, with multiple applications ranging from magnetic resonance imaging (MRI) contrast agents to magnetic hyperthermia, magnetic guiding (tumour homing) and magnetically triggered drug delivery.[1] Most of the clinically relevant nanoparticles for theranostics are magnetic field responsive iron oxide-polymer composites.[2] Several studies in the recent literature reported evidence that the temperature can locally reach several tens of Kelvin (K) above the solvent or gas phase temperature in the close vicinity of magnetic nanoparticles subjected to either a radiofrequency (RF) magnetic field or an intense laser beam (plasmonic resonance). Pellegrino and coworkers recently grafted a fluorescent dye onto magnetic nanoparticles through a thermocleavable bond and a polymeric spacer.[3] By comparing the level of fluorescence in the supernatant over time under a RF magnetic field to a calibration curve obtained by heating in a thermal bath, they precisely estimated the local

temperature. They also determined a temperature *vs.* distance profile in the nm range using polymer spacers of increasing lengths. Since then, several groups have reported other evidence of high temperature gradients at NP surfaces using other chemical reactions or phase transitions such as a retro Diels-Alder reaction,[4] double-stranded DNA melting,[5] expression of a heat-shock protein gene promoter,[6] or heterogenous catalysis of the Fischer-Tropsch reaction.[7] All of these studies reported the detection, in "cold" conditions, of products normally produced only at significantly elevated temperatures. For example, the enzymatic reactions would require temperatures of 313-323 K whereas 373-423 K would normally be required for the rearrangements of organic molecules. Therefore, it was deduced that in the close vicinity of the surface of magnetic or plasmonic NPs, temperatures much higher than the medium could be reached, possibly higher than the boiling temperature of solvent, at least transiently.

Recently, molecular dynamics (MD) simulations of thermosensitive polymer chains grafted onto the surface of plasmonic particles showed that a temperature as high as 410 K can be maintained during several picoseconds at a gold/water interface grafted with thermosensitive polymers, acting as a thermal barrier.[8] The same commercial thermosensitive copolymers called Jeffamine™ exhibiting a lower critical solution temperature (LCST) in water were also grafted onto iron oxide NPs to study the variation of their relaxometric properties and to design thermosensitive MRI contrast agents[9]. The present work also makes use of such thermal transitions (LCST) of polymer chains grafted on iron oxide NPs. A sol-gel route and copper assisted azide-alkyne cycloaddition ("click") chemistry were used for the grafting poly[2-(dimethylamino)ethyl methacrylate] (PDMAEMA) onto iron oxide NPs. This is a thermo- and pH-sensitive polycation that has been used in applications such as antibacterial surfaces.[10] However, unlike most previous studies based on the release of a probe that was read after the magnetic hyperthermia treatment and compared to a calibration curve, in this article the variation of hydrodynamic diameter of magnetic thermosensitive NPs was assessed directly by dynamic light scattering performed *in situ* during the application of the RF magnetic field. This study therefore introduces a new method to study the thermal behavior of thermogenic NPs under electromagnetic excitation (be it light or a magnetic field) in real time (as opposed to off-line).

2. Materials and chemical syntheses

2.1 Chemicals

Iron dichloride tetra-hydrate powder ($FeCl_2{\cdot}4H_2O$), iron tri-chloride hexa-hydrate 45% solution ($FeCl_3{\cdot}6H_2O$), ammonia 28% solution (NH_4OH), diethyl ether ($(C_2H_5)_2O$), hydrochloric acid 37% solution (HCl), nitric acid 69% solution (HNO_3), acetone ($(CH_3)_2CO$), iron (III) nitrate powder ($Fe(NO3)_3$), sodium azide 99.5% (NaN_3) were provided by Sigma Aldrich. Water used was MilliQ™ (18MΩ·cm conductivity). 3-(2-aminoethylamino)propyltrimethoxysilane 96% (AEAPTMS), N-hydroxysuccinimide (NHS) and NHS-Fluorescein were purchased from Alfa Aesar. Reagent grade anhydrous diethyl ether was from Baker. Bromoacetic acid, 1-ethyl-3-3-dimethylaminopropyl carbodiimide hydrochloride (EDC), diisopropylethylamine (DIPEA), ethylenediaminetetraacetic acid (EDTA) were from Acros Organics. Polystyrene latexes were from Polysciences. For the synthesis of PDMAEMA, propargyl-2-bromoisobutyrate (PBiB), 2-(dimethylamino)ethyl methacrylate (DMAEMA), tin(II) 2-ethylhexanoate ($Sn(EH)_2$) were purchased from Sigma Aldrich. Tris-(2-pyridylmethyl)amine (TPMA)[11] and its copper(II) complex[12] were prepared as previously reported. *N*,*N*-Dimethylformamide (DMF), reagent grade, was purchased from Caledon and used as received. The monomer DMAEMA was passed through a column of basic alumina immediately prior to polymerization to remove the inhibitor.

2.2 Synthesis of propargyl-terminated PDMAEMA by Atom Transfer Radical Polymerization (ATRP)

The polymer chains were grown by ATRP controlled radical polymerization with the activator regenerated by electron transfer (ARGET) catalytic system where the initiator (copper I complex) is generated by electron

transfer (redox reaction between Cu^{2+} and Sn^{2+}),[13] as depicted in Figure S1(A). In a 100 mL round bottom flask, the monomer (10.0 g DMAEMA, 10000 eq.), the alkyne-functionalized initiator (0.065 g PBiB, 50 eq.), and the catalyst (0.33 mL Cu(TPMA)Br_2, 1 eq.) were mixed in DMF (7.5 mL), to produce a solution of 60% monomer content by mass, with a copper content of 115 ppm. Nitrogen gas was bubbled through the mixture at room temperature for 30 minutes to remove oxygen, then the solution was heated to 60°C, and $Sn(EH)_2$ (0.41 mL, 0.1 g·mL^{-1} in toluene, 10 eq.) was added to initiate the polymerization. A small flow of nitrogen gas was maintained during the polymerization. After 3 hours the polymerization was cooled and opened to the atmosphere. The solution was dialyzed against water (2 L) using a Spectra/Por regenerated cellulose membrane with a molecular weight cut-off (MWCO) of 2 kDa (Spectrum Laboratories). The resulting aqueous solution was then lyophilized to yield the final polymer as a white solid. The polymer ^{1}H NMR spectrum (in $CDCl_3$, 400 MHz) is provided in Figure S1(B): δ 4.61-4.58 ppm (multiplet (m), 2 protons (H)), 3.95-4.05 ppm (broad (br), 196 H), 2.49-2.61 ppm (br, 198 H), 2.23-2.27 ppm (br, 599 H), 1.70-2.00 ppm (br, 180 H), 0.80-1.05 ppm (m, 280 H), degree of polymerisation *DP*=98. The SEC chromatogram (Figure S1(C)) yields a molar mass distribution: Weight average molecular weight (M_W) = 12.7 kDa, Dispersity ($Đ$) = 1.29.

2.3 Synthesis of iron oxide NPs

Superparamagnetic iron oxide NPs were synthesized according to Massart's alkaline co-precipitation of ferrous and ferric chloride salts in water.[14] The magnetite (Fe_3O_4) NPs obtained were further oxidized into maghemite (γ-Fe_2O_3) by treatment with a boiling $FeNO_3$ solution, giving after several washings with acetone to remove excess ions, a dispersion of superparamagnetic NPs stable in a pH range 1.5-2.5, *i.e.* remaining in a monophasic state under the application of a magnetic field of arbitrary value. A size sorting procedure was then applied, as described in the supporting information and in previous work:[15] it is based on the screening of the electrostatic repulsions between NPs by excess addition of electrolyte (here HNO_3). The two phases were then separated over a strong ferrite permanent magnet (Calamit™). The concentrated bottom phase (referred to as C) was enriched in larger NPs while the upper dilute supernatant (reffered to as S) contained on average smaller NPs. Proceeding this way multiple times, different fractions were obtained, among which S1S2, C1S2, C1C2 with increasing average sizes respectively 6-7 nm, 10-12 and 10-15 nm according to TEM analysis.

2.4 Aminosilane modification of the surface

3-(2-Aminoethylamino)propyltrimethoxysilane (AEAPTMS, 530 µL, 2.4 mmol, representing an excess, 20 molecules per nm^2 for S1S2) was grafted on the surface of the NPs (420 mg, 5.25 mmol of Fe), in a mixture of solvents (10% water 90% ethanol) in acidic conditions (arising from the low pH of the ferrofluid) at first to hydrolyse the alkoxysilane into a hydroxysilane, followed by condensation with the Fe-OH moieties of iron oxide in neutral conditions for an hour, and boiling at reflux for another hour, a protocol adapted from Duguet and Mornet's patent.[16] The sample was then washed multiple times with methanol by a precipitation-redispersion process before being redispersed in water with a pH adjusted to 3 with dilute HNO_3. The number of available primary and secondary amines at the surface of the NPs was determined through the grafting of a large excess of NHS-fluorescein in water at neutral pH. The excess was washed several times with Amicon™ centrifuge tubes with a 30 kDa membrane and water acidified at pH ~5 until the filtrate did not show fluorescence. The amide covalent bonds between grafted fluorescein molecules and NPs were then hydrolysed overnight at pH 2. The NPs were separated from the solution, the pH was set to 5 and the fluorescence was measured and compared to a calibration curve (see Supporting Information).

2.5 Synthesis of the cross-linker

Azidoacetic acid (AZ) was synthesized following a modified procedure from Srinivasan et al.[17] Sodium azide NaN_3 (107 mmol) was dissolved in 30 mL of distilled water and cooled down with an ice bath. Bromoacetic acid (51 mmol) was then added slowly and the mixture was let to warm to room temperature overnight. The

chemical obtained *via* substitution was protonated by acidification and extracted in diethyl ether, dried over $MgSO_4$ and finally, after the solvent was removed at 40°C under reduced pressure, a pale yellow oily liquid was obtained. FT-IR (Fig. 2b-spectrum C) and ^{1}H NMR (Fig. S2) agreed with previously reported data.[17]

2.6 Grafting of the cross-linker onto the NPs

Typically 1 eq. of azidoacetic acid (0.83 mg, 8 μmol) with respect to primary amines was added to the NP aqueous suspension (12 mg, 75 μmol Fe). 2 eq. of EDC (3.14 mg, 16 μmol) and 1 eq. NHS (0.94 mg, 8 μmol) were then added and the pH was adjusted to 5. An "activated" NHS ester was produced *in situ*, reacting with the primary amines at the surface of the iron oxide NPs to form amide bonds. The mixture was allowed to react for 6 h and dialyzed against 5 L of milliQ™ water.

2.7 "Click" reaction to couple the PDMAEMA chains with the NPs

Typically 1 eq. of propargyl-terminated PDMAEMA (82 mg, 8.2 μmol), 2 eq. of ascorbic acid (3.3 mg, 16.4 μmol), and 0.5 eq. of $CuSO_4$ (0.65 mg, 4.1 μmol) were added to the NPs (12 mg, 75 μmol of Fe) functionalized with the clickable azido moiety (by the previous step) in DMF. The mixture was let to react overnight and dialyzed against 5 L of a 10 mM EDTA solution to complex and remove the copper salts, followed by pure water.

3. Instrumentation methods

3.1 Proton nuclear magnetic resonance spectroscopy (^{1}H NMR)

^{1}H NMR spectra were obtained at 400 MHz on a Varian Inova spectrometer and calibrated according to the residual solvent signal of $CDCl_3$ (7.26 ppm).

3.2 Size Exclusion Chromatography (SEC)

SEC was carried out with a Waters 515 HPLC pump using two PLgel mixed-D columns (5 μm pore size) in series, with a Wyatt Optilab rEX refractive index detector. DMF with 1% NEt_3 and 10 mM LiBr was used as the eluent, the temperature of the columns was maintained at 85°C, and the flow rate was 1.0 mL·min^{-1}. Molecular weight was determined relative to poly (methyl methacrylate) (PMMA) standards.

3.3 Infrared (IR) spectroscopy

IR spectra were acquired on a Nicolet iS10 FT-IR spectrometer with a diamond Smart iTX tool and analyzed with the Omnic 9.0 software. Samples dispersed in water were dried over the ATR crystal and measurements were performed with 32 scans.

3.4 Transmission electron microscopy (TEM)

TEM was performed on a Hitachi H7650 microscope operated at 80 kV on samples deposited at mass concentrations of 1 g·L^{-1} onto copper grids by a lab-made spraying tool, and images were acquired on an ORIUS SC1000 11MPx Camera. Selected area electro-diffraction (SAED) patterns were imaged at the Fourier plane of the microscope.

3.5 Magnetic hyperthermia (MH)

Various colloidal NPs (magnetic, magnetic and thermosensitive, and neither magnetic nor thermosensitive) were submitted to a radiofrequency magnetic fluid with a Seit Elettronica Junior™ induction soldering machine. The 3 kW MOSFET solid state resonant circuit produces a quasi-sinusoidal alternating magnetic field at a radiofrequency f=755 kHz in the induction coil (4 turns of 55 mm outer diameter, spaced every 10 mm, refrigerated by internal cold water circulation, Figure 1). The RMS field amplitudes H_0 were varied

between 2.7 and 6.4 $kA \cdot m^{-1}$ for durations of 15 min to induce heat generation by the NPs. The macroscopic temperature of the sample was measured by a fibre optic sensor with a diameter of 420 µm (OTG-M420, Opsens™, Québec city, Canada) passed through a hole in the cap of a semi-micro polystyrene cuvette filled with 1 mL sample (closed to prevent solvent evaporation). In a standard experiment, the temperature first increased linearly with time, then reached a plateau corresponding to perfect compensation of the heat powers respectively generated by the sample and dissipated into the surrounding medium. Between consecutive field applications, the sample was left to rest for 15 minutes, allowing the return to room temperature through thermal losses.

3.6 Dynamic light scattering

Two kinds of instruments were employed for the assessment of the hydrodynamic diameters by dynamic light scattering (DLS) at varying temperatures. Off-line DLS and phase analysis light scattering (PALS) measurements were performed on two Zetasizer™ NanoZS instruments (Malvern, UK) operating at scattering angles of respectively 90° and 173°. They enabled measurement of the *Z*-average hydrodynamic diameters (D_h), polydispersity index (PDI) and Zeta potential of the NPs (using the Smoluchowski approximation). The measurements were performed in dilute polymer solutions in water (3 to 20 $g \cdot L^{-1}$) to measure the LCST of free chains. The different suspensions of NPs were measured at ~0.1 $g \cdot L^{-1}$ iron oxide, at controlled pH. Reported D_h and PDI values were measured in triplicate from the 2nd order cumulant fit of the correlograms obtained from the light intensity scattered at 90°. Samples were held in 100-QS quartz cells (1 cm path, 4 transparent walls) from Hellma Analytics for size measurement during temperature ramps. For both angles, an equilibration time of 120 s was set before each measurement to reach thermal equilibrium. The temperature was then varied from 15 to 50°C separated by steps of 0.5°C, and the *Z*-average and derived count rates were recorded. The results obtained at the two angles on the NanoZS instruments were similar.

In situ measurements were acquired simultaneously during the magnetic field application using the VASCO Flex™ remote-head DLS instrument developed by Cordouan Technologies.* The principle is based on light scattering detected by fibre optics in backscattering conditions,[18] enabling measurements of concentrated samples (here 1 $g \cdot L^{-1}$ of iron oxide). The scattering volume is defined at the intersection between the incident measurement beam (horizontal) and the alignment beam (tilted at an angle) and the measurement distance is adjusted to 8 cm compared to the remote head (Figure 1a). Kinetic DLS measurements were acquired with the NanoQ™2.5 software. The remote head was adjusted to locate the scattering volume approximately 2 mm behind the wall of the cuvette. The beam power was tuned to read a scattered intensity in the working range 1000-4000 kcps of the detector. After choosing the minimum decay time and number of channels of the correlator, the acquisition was launched for an unlimited time with independent sub-runs of 20 seconds. The correlogram of each sub-run was analysed on the fly by both the 2nd order cumulant and Pade-Laplace methods. The temperature was recorded at a rate of 50 Hz all along the experiment by the Opsens conditioner (through RS-232 cable) and at a rate of 1 Hz by the NanoQ™2.5 software (through an analogous output, with a shielded cable to protect it from the electromagnetic perturbations when the RF magnetic field was on).

3.7 Combined MH and DLS

As any metallic part located too close to the solenoid would be heated through eddy currents generated by the electrical field component of the RF excitation, the magnetic field intensity in front of the coil (outside) was estimated to predict how it decays with distance. A scout coil of diameter 1.75 cm (of surface S=2.4 cm^2) was used to estimate the magnetic field strength, generating a RMS electromotive force $e_{RMS} = B_0 \times S \times 2\pi f$

* This commercial instrument was developed within the SNOW FP7-NMP-2010-SME-4 European project dedicated to *in situ* characterization of nanoparticles in either harsh environments or combined with another technique (*e.g.* small angle X-ray scattering) for quality control of nanomaterials production.

when submitted to a RMS field induction B_0, detected by an oscilloscope (Teledyne LeCroy Waveace™ 102). A magnetic induction B_0=16.3 mT was measured at a distance of 5 cm from the entry, B_0=14.1 mT at 15 cm, B_0=1.28 mT at 22 cm, and B_0=0.44 mT at 30 cm, in accordance with studies showing the field intensity decay *versus* distance for such magnetic induction setups.[19] In practice, the field intensity was still strong at a distance of 8 cm between the closest part of the remote head and the coil, therefore the generator was used at a maximum of 60% of its maximum power (B_0=8 mT, H_0=6.3 kA·m^{-1}) in order to minimize the parasitic heating of metallic parts inside the remote head. The field lines were also calculated using cylindrical axi-symmetry with the finite element simulation freeware FEMM (http://www.femm.info), which showed calculated field values close to the experimentally measured ones (Figure 1b). For the control experiment under a static (DC) magnetic field, the sample holder was placed inside a solenoid with 1000 turns (8.75 Ω) fed by a current from a DC generator (Française d'Instrumentation), the field intensity being measured with a Hall-effect probe (Lakeshore 425 gaussmeter).

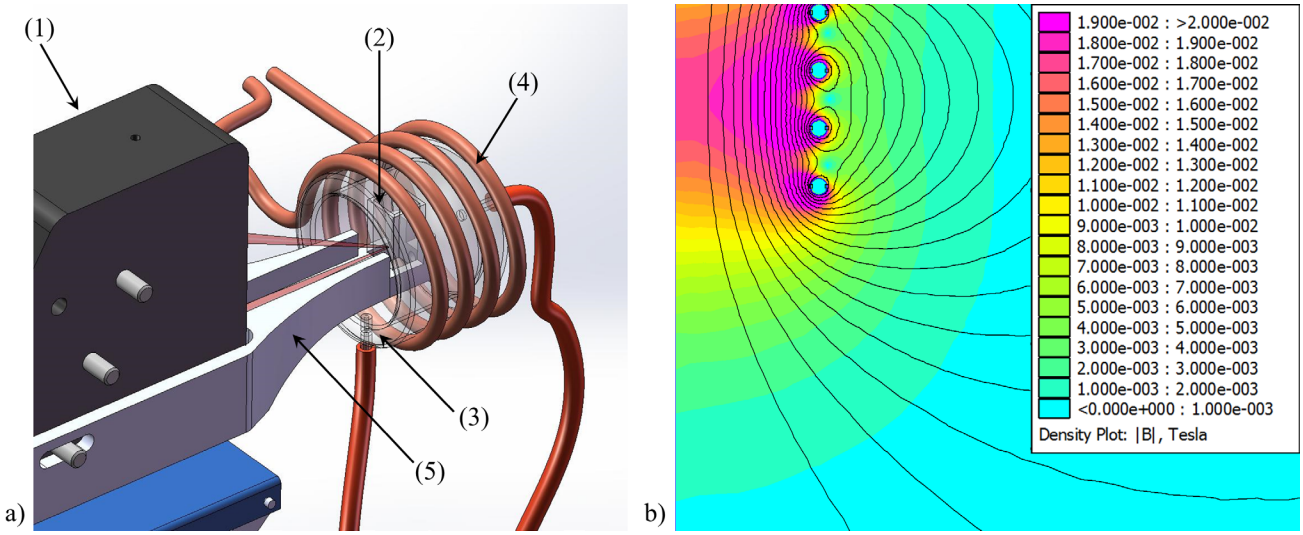

Figure 1: a) Illustration of the simultaneous DLS/magnetic hyperthermia experiment. The remote head (1) of the Vasco Flex™ backscattering setup is located ~8 cm from the quartz cuvette (2) placed in a glass water-jacket (3) inside the 4-turn coil of 55 mm outer diameter (4). The stage (5) maintains the optical path constant and holds the cuvette inside the coil. It was made by 3D printing from a plastic material (insensitive to eddy currents). The radiofrequency power generator operating at f=755 kHz creates a maximum induction B_0=16.3 mT as measured by a scout coil and b) as calculated by a finite element model simulation for an AC current of 234 Amps. For combined DLS/MH experiments, the magnetic induction was held at a maximum value B_0=8 mT (field strength H_0=6.3 kA·m^{-1}) to avoid parasitic heating of metallic parts inside the remote head.

3.8 Relaxometric properties

A NMS120 Minispec™ NMR analyzer from Bruker (20 MHz or 0.47 T) was used to investigate the effect of the superparamagnetic iron oxide NPs on relaxation times of hydrogen nuclei of surrounding water to test their efficiency as MRI contrast agents. After perturbing the system of nuclear spins out of equilibrium through a RF pulse sequence, the recovery of the longitudinal (M_z) and transverse (M_{xy}) components of the proton magnetization over time occur with characteristic decay times of T_1 (spin-lattice relaxation) and T_2 (spin-spin relaxation) respectively. Recommended protocols were applied to measure them accurately.[20] For T_1, an inversion recovery sequence was applied starting from an initial inversion delay of 10 ms, with a series of 15 to 20 acquisition points increased by a factor of 1.4 relatively to the previous one, a gain of 80 dB, and 3 scans separated by a recycle delay (RD) of 5 s. The number of acquisition points was adjusted to record the relaxation curve during approximately 5T_1. To determine T_2, a Carr-Purcell-Meiboom-Gill (CPMG) sequence was applied with spin-echo times in a range from 0.3 to 3 ms, a gain of 72 dB, 200 points of acquisition and 10 scans with RD=5 s. Spin-echo times were adjusted to insure that the observation time exceeds 3T_2. The

exponential decay curves were analysed with the CONTIN eigenfunction expansion method to derive the relaxation times of samples at increasing concentration. Typically, the measured relaxation times varied in a range from ~8 ms (T_2 at 0.70 mM_{Fe}) to ~600 ms (T_1 at 0.175 mM_{Fe}). As usual in the literature of MRI contrast agents, the decay rates were then plotted *vs.* concentration expressed in equivalent iron concentration [Fe] in mM, and the linear regression gave a slope equal to the relaxivity value, which characterizes the efficiency of a magnetic NPs contrast agent either for positive (T_1) or negative (T_2) contrast.

$$\frac{1}{T_{1,2}} = \frac{1}{T_{1,2}^{H_2O}} + r_{1,2} \times [Fe]$$

[Fe] equivalent iron concentration (mM_{Fe})
$r_{1,2}$ relaxivity ($s^{-1} \cdot mM_{Fe}^{-1}$)
$T_{1,2}$ relaxation time of M_z or M_{xy} of water in presence of the contrast agent (s)
$T_{1,2}^{H_2O}$ relaxation time of M_z or M_{xy} of pure water (s)

As the samples are thermosensitive, they were equilibrated at varying temperatures between 15°C and 50°C by 5°C steps with a regulated circulating bath (Huber Polystat™ CC, Offenburg, Germany). At each temperature, both T_1 and T_2 relaxation times were measured for concentrations of 0.70, 0.35 and 0.175 mM_{Fe}.

4. Results and discussion

The aim of this study is to demonstrate the fast responsivity of magnetic and thermosensitive NPs to a RF alternating magnetic field through a combination of magnetic hyperthermia and dynamic light backscattering experiments in a simultaneous fashion and comparison to other dynamic but off-line measurements (dynamic light scattering and proton relaxometry).

4.1 Synthesis of the iron oxide NPs and polymer grafting

To achieve the goal of *in situ* probing of thermosensitive magnetic NPs, the synthesis of well-defined NPs with adequate properties was mandatory. First, superparamagnetic NPs were synthesized using an alkaline co-precipitation procedure in water followed by an electrolyte-mediated magnetic sorting procedure described in the supporting information. The procedure for grafting of the thermosensitive PDMAEMA chains is illustrated in Figure 2a. The original NPs exhibit hydroxyl functionalities (Fe–OH) at their surfaces, allowing the grafting of AEAPTMS by sol-gel chemistry (hydrolysis-condensation). The amino groups on the grafted silanes were then coupled to the carboxylic acid groups of azidoacetic acid using an NHS-mediated EDC coupling. Finally, the alkyne-terminated PDMAEMA was conjugated to the azides by a copper-mediated azide-alkyne cycloaddition reaction.

The grafting steps were assessed by attenuated total reflectance infrared (ATR-IR) spectroscopy (Figure 2b). The spectrum of the original ferrofluid presents peaks in the 3000-3500 cm^{-1} range attributed to stretching vibrations of water. The peak at 1392 cm^{-1} is ascribed to elongation modes of adsorbed NO_3^- ions. The peak at 1627 cm^{-1} is ascribed to the bending vibration of water, and the large, strong peak starting at 536 cm^{-1} corresponds to the stretching vibration of the bond between oxygen and iron. This is explained by the hydration of the sample by remaining traces of water. This water is superficial rather than interstitial as there is evidence from TEM analysis (see Figure 1c for an example of an electron micrograph) that the NPs consist of single crystals with no visible defects, as also proved by their electron beam diffraction pattern (Figure 1d). The signal from the Fe-O bond ensures the presence of hydroxyl groups on the surface of the NPs, which are thereafter exploited as anchor groups for the silanization and subsequent functionalization. After grafting of AEAPTMS, new signals appear in the IR spectrum.

Peaks at 1114 and 1043 cm^{-1} are due to the stretching of C–N bonds and Si–O–Si bonds. Peaks at 2926 and 2853 cm^{-1} correspond to the stretching of $–CH_3$ and $–CH_2–$ groups. The other peaks were already present before the reaction. These observations are consistent with the grafting of AEAPTMS, which exhibits

aliphatic carbons and primary ($–NH_2$) and secondary (–NH–) amines. There is no sign of alcohol groups, which suggests the conversion of the alkoxysilane into a silanol followed by chemical bonding with the hydroxyl groups on the surface of the NPs is complete. Azidoacetic acid was grafted on the primary amines through an amide bond formation as a next step toward the synthesis of the thermosensitive NPs. The IR spectrum remains roughly unchanged, but exhibits a strong sharp peak at 2015 cm^{-1} which is typical of an azide functional group. The spectrum shows broad bands ascribed to amide carbonyl groups in the 1650–1690 cm^{-1} range (amide band I for C=O, amide band II for N-H). Finally, the grafting of PDMAEMA results in a more complex spectrum. There is only a weak residual azide peak, which suggests substantial conversion during the reaction. There is also a strong peak at approximately 1750 cm^{-1}, which likely corresponds to the carbonyl stretch of an amide and peaks in this region are generally broader and stronger than in the previous spectrum. The peaks at ~2500 cm^{-1} correspond to amines or amine salts of the polymer.

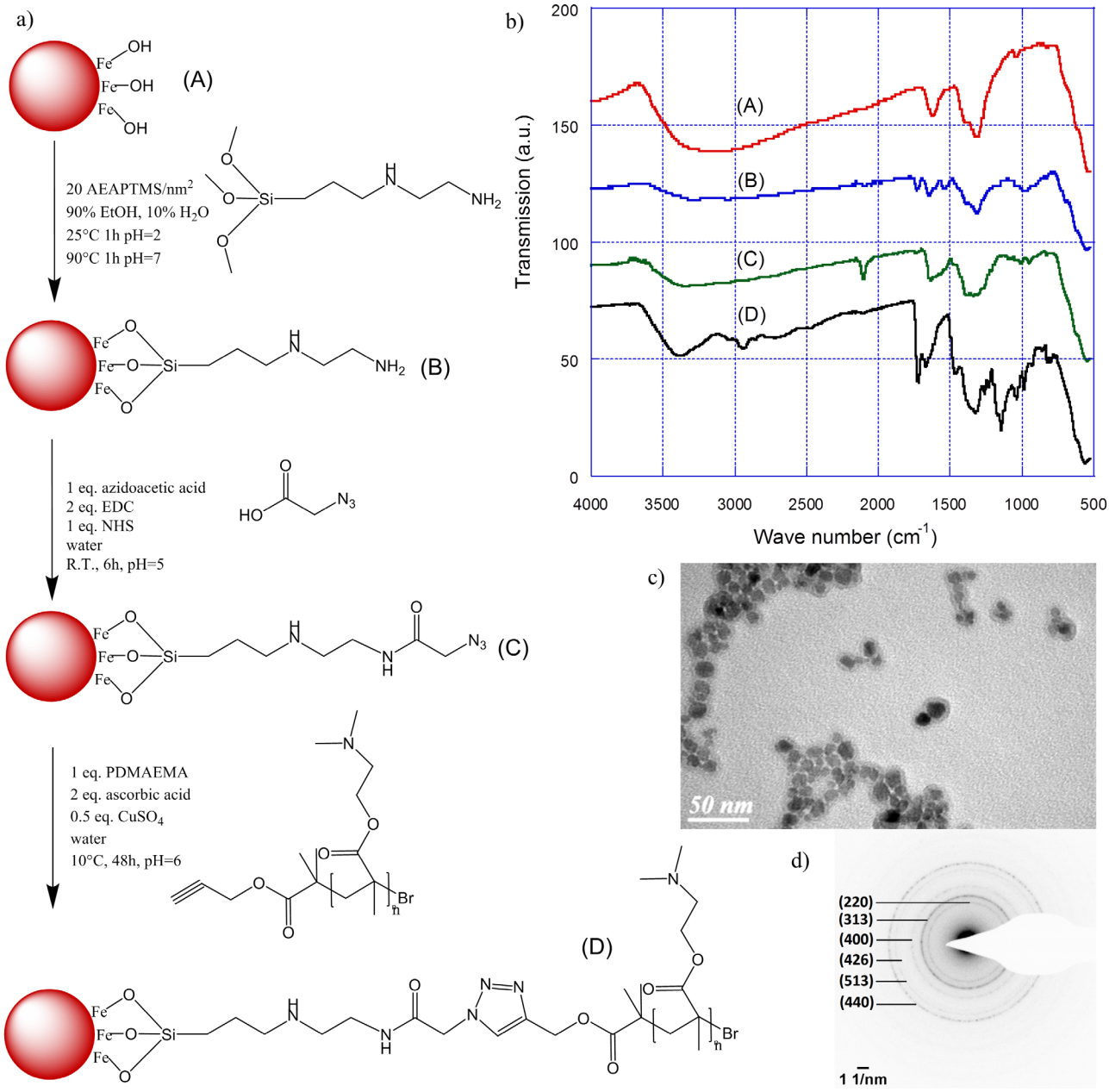

Figure 2: a) Scheme showing the successive reaction steps to build the magnetic thermosensitive NPs: (A) Original maghemite (γ-Fe_2O_3) iron oxide NPs; (B) A sol-gel reaction with the AEAPTMS organosilane primary to introduce primary amines (γ-Fe_2O_3@AEAPTMS NPs); (C) After grafting of the azide (γ-Fe_2O_3@AEAPTMS-AZ NPs); (D) Final

γ-Fe_2O_3@AEAPTMS-AZ-PDMAEMA NPs coated by the polymer chains. b) ATR-IR spectra of the reaction products A-D; c) A TEM image showing S1S2@AEAPTMS-AZ-PDMAEMA NPs clearly exhibiting core-shell structure. d) The selected area electron diffraction provides evidence that the S1S2 cores are crystalline. The Bragg peaks measured by SAED are assigned to the Miller indices of the atomic planes of the maghemite phase.

4.2 Solution properties of the PDMAEMA chains

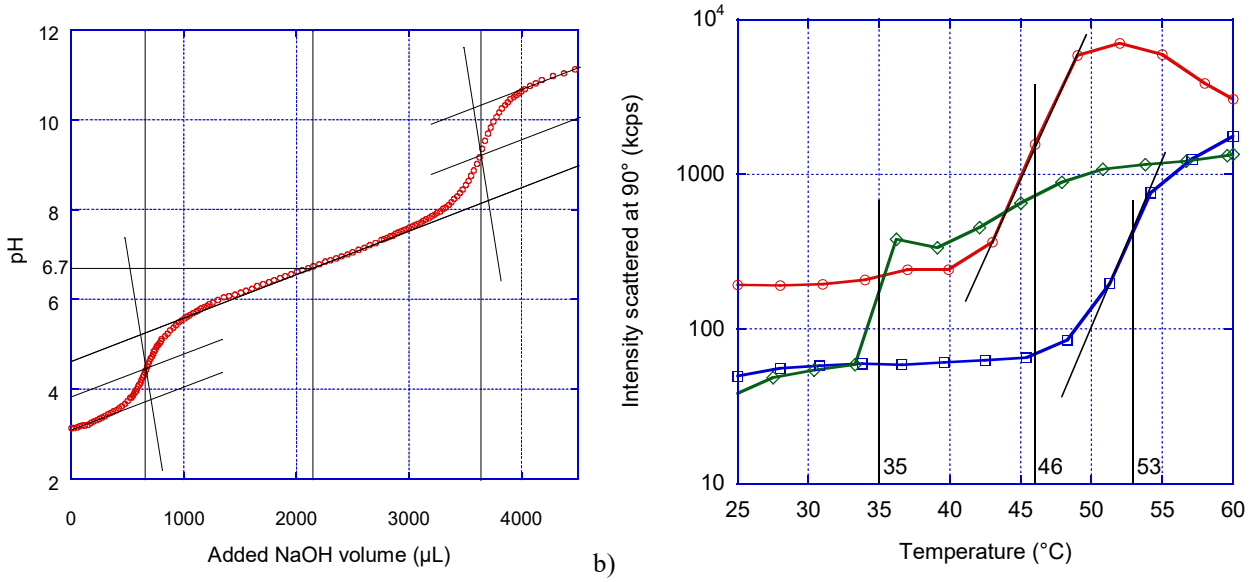

Figure 3: a) pH-metric titration of PDMAEMA chains by NaOH (0.3 M) for the determination of the pKa=6.7 of the secondary amines moieties; b) Determination of the cloud point of PDMAEMA by DLS at 90° in solutions at 35°C at a concentration of 3 mg·mL^{-1} at pH 5 (diamonds), near 53°C for 10 mg·mL^{-1} at pH 7 (squares), and 46°C for 20 mg·mL^{-1} at pH 7 (circles). The decrease in scattered light intensity for temperatures above 50°C for 20 mg·mL^{-1} at pH 7 denotes a macroscopic phase-separation (coacervation) and sedimentation.

The solution behaviour of PDMAEMA chains in water is known to be both thermo- and pH-sensitive. Tertiary amines of the PDMAEMA chains are characterized by their respective value of the logarithmic constant of dissociation (pKa). From the Henderson-Hasselbalch equation, it is possible to plot the relative percentages of both species, depending on the pH. At pHs lower than their pKa, amines are protonated, whereas they are unprotonated and uncharged at pHs higher than the pKa of 6.7, as determined by acid-base titration (Figure 3a). This pKa value appears relatively lower than usual for amines, but the proximity of charges along a polymer backbone is not thermodynamically favourable, and lowers the pKa of PDMAEMA.

It is also known from its Flory-Higgins phase diagram that PDMAEMA chains become insoluble in water above their cloud point and that this cloud point becomes lower when the polymer concentration increases, tending towards a limit called the "lower consolute transition temperature" or "lower critical solution temperature" (LCST). In the case of PDMAEMA, the cloud point critically depends not only on concentration but also on pH[21] and on the polymer length and architecture (linear *versus* branched chains).[22] Figure 3b illustrates this variation of the cloud point at different values of concentration and pH, either below (pH 5) or near (pH 7) the pKa of the amines.

4.3 Colloidal and charge properties of the magnetic core-polymer shell NPs

Laser PALS velocimetry is an effective way to estimate the sign and intensity of the charge at the surface of NPs by the readout of the Zeta potential, deduced from the electrophoretic mobility by the Smoluchowski equation. In the double-layer model of charged colloids, the Zeta potential is defined as the electric potential interface at the stationary layer, *i.e.* the shear plane inside the solvent in the motion of the NP relative to

solvent under the action of the electromotive force. Charged particles are better dispersed in water because they bear charges of the same sign and thus exhibit repulsive interactions between each other. It is commonly accepted that an absolute value |Zeta|=25 mV sets the limit between minimally and highly charged particles. Pristine iron oxide NPs bear hydroxyls at their surfaces and are uncharged at neutral pH, meaning that the isoelectric point of this amphoteric material is pH~7.5 (equal number of $Fe–O^-$ and $Fe–OH_2^+$ species). The iron oxide surface bears a positive charge in acidic media and negative charge in basic media. However, in practice, to obtain |Zeta|>25 mV and stable uncoated iron oxide colloids, the pH has to be lower than 4 or higher than 10, while the ionic strength needs to remain limited, typically less than 20 mM, otherwise the electrostatic repulsions are screened by the electrolyte. Zetametry is a powerful tool to investigate the nature of the chemical functions grafted on the NPs, first the primary and the secondary amines of the aminosilanes, and then the tertiary amines of the polymer chains. Measurements of the Zeta potential *versus* pH for all of the coated NPs (Figure 4) show that the isoelectric point is the highest (pH~10) for the γ-Fe_2O_3@AEAPTMS NPs, while it decreases by one unit (pH~9) for the final γ-Fe_2O_3@AEAPTMS-AZ-PDMAEMA NPs. As predicted, amine moieties lose their positive charge above the pKa, and the remaining negative charges must arise from still uncoated hydroxyl groups $Fe–O^-$ or possibly from deprotonation of the N–H groups of the secondary amine or amide associated with the AEAPTMS linker.

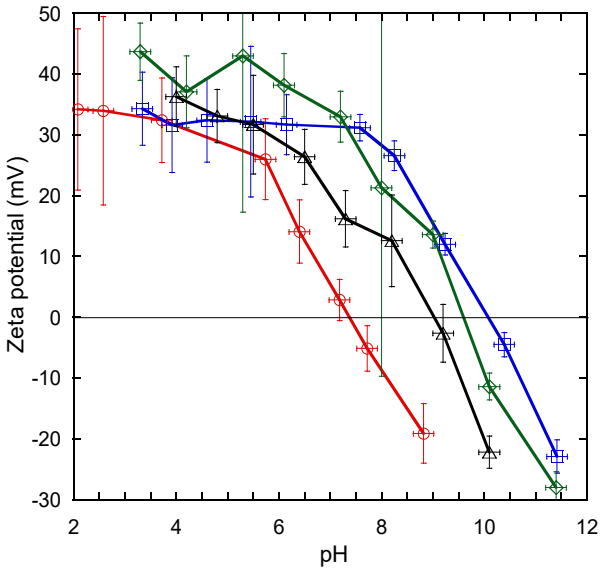

Figure 4: Zeta potential *vs.* pH for acidic γ-Fe_2O_3 NPs (circles), aminosilane grafted γ-Fe_2O_3@AEAPTMS NPs (squares), cross-linker grafted γ-Fe_2O_3@AEAPTMS-AZ NPs (diamonds) and finally thermosensitive γ-Fe_2O_3@AEAPTMS-AZ-PDMAEMA NPs (triangles). PDMAEMA-coated NPs are charged over the whole acidic pH range up to pH=6.5.

Compared to bare NPs, grafted NPs exhibit higher stability over a broader pH range because pure electrostatic repulsions are replaced by electro-steric repulsions, meaning that the organic chains at short distances cannot interpenetrate, leading to better dispersed NPs. The shift of the isoelectric point along the successive grafting steps can be ascribed to variation in the quantity of amines at the surface of the NPs. The grafting of azidoacetic acid on the primary amines reduces the isoelectric point of the NPs by approximately 0.5 pH units, because the azide function is neutral at all pHs. Finally, the isoelectric point is further reduced by 0.5 pH units following grafting of PDMAEMA chains onto the NPs using the azido moieties as anchor groups. This observation is consistent with the pKa value of PDMAEMA that has been determined to be 6.7 by acid-base titration (Figure 3a). In addition, for a brush of PDMAEMA chains grafted at high density on NPs such as in the current system, a curvature effect can further decrease the pKa, as previously reported for star-like PDMAEMA micelles.[22]

4.4 Temperature ramps to monitor the variation of hydrodynamic size by DLS

Figure 5 shows the variation of the derived count rate of scattered light and of the *Z*-average diameter of polymer-grafted NPs over varying temperatures. Like PDMAEMA chains in solution, the shell of the grafted-NPs, mainly composed of this polymer, dehydrates at elevated temperature, resulting in a variation of both their scattered light intensity and hydrodynamic diameter. However, unlike polymer chains in solution, which usually exhibit an abrupt transition over a narrow range of temperatures (defining the "cloud point", as on Figure 3b), for these thermosensitive nano-objects the variation appears continuous and spans a broader range of temperatures. Nevertheless, a transition temperature can still be deduced from the inflection point of the scattered light intensity *versus* temperature curve. This inflection point is located between 30 and 35°C for the three grafted-NPs represented in Figure 5a, which is close to the cloud point determined at 35°C on a solution of PDMAEMA chains at 3 mg·mL^{-1} in pH 5 buffer (Figure 3b). It is also close to the value of 38°C reported in literature[21] for chains PDMAEMA of similar length (*DP*=85) at 1 mg·mL^{-1} but above the pKa (pH=11). Therefore it can be concluded that the thermal transition of the chains grafted at the iron oxide surface have a direct influence on the colloidal state of the core-shell NPs.

Usually an increase in derived count rate accompanies an increase of hydrodynamic diameter, the scattered intensity being proportional to the sixth power of the size of the NPs (or aggregates) in the Rayleigh approximation. However, the present samples did not show any sign of aggregation and the evolution of hydrodynamic diameter with temperature was different depending on the iron oxide core sizes. It decreased by ~10 nm for S1S2 between 15 and 50°C, increased by ~10 nm for C1S2, and remained almost constant for C1C2. In comparison, the bare S1S2 cores without the thermosensitive shell exhibited both constant scattered intensity and hydrodynamic diameter over the whole temperature range. The increase in derived count rate for all the polymer-grafted NPs is tentatively explained by the dehydration of the outer shell, resulting in stronger light scattering contrast and a higher intensity collected at either 90° or 173° from the incident laser beam.

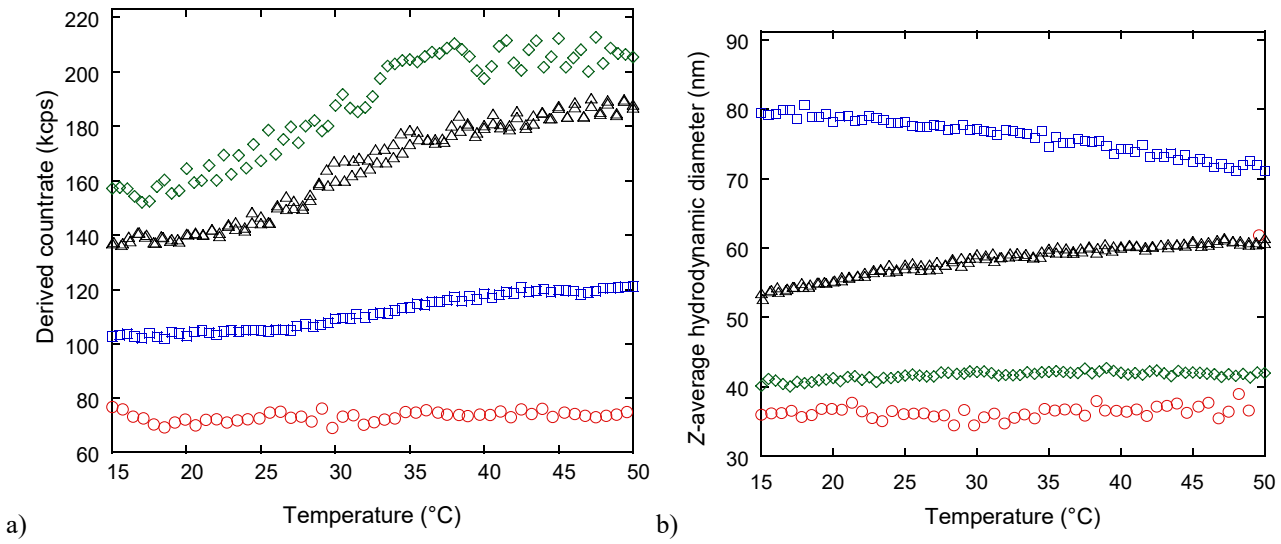

Figure 5: Off-line DLS results on bare acidic S1S2 NPs (circles), and on three batches of AEAPTMS-AZ-PDMAEMA-grafted NPs differing by the inorganic core sizes (~0.1 g·L^{-1} iron oxide): S1S2 (squares), C1C2 (diamonds) and C1S2 (triangles). The scattered intensity (a) and the *Z*-average diameter (b) are plotted *versus* temperature. The pH was adjusted to 5.3 (below pKa of PDMAEMA) to maintain the NPs well dispersed while still exhibiting a LCST behaviour.

4.5 Thermosensitive relaxometric properties

Water proton relaxivity measurements were performed at different temperatures from 10 to 50 °C for samples containing uncoated S1S2 superparamagnetic NPs and S1S2@AEAPTMS-AZ-PDMAEMA coated-NPs.

This document is the Accepted Manuscript version of a Published Work that appeared in final form in *J. Phys.* D: *Appl. Phys.* 48 (2015) 494001 © Institute of Physics (UK) after peer review and technical editing by IOP Publishing. To access the final edited and published work see http://dx.doi.org/10.1088/0022-3727/48/49/494001

Figure 6 shows a comparison of the results and the effect of the thermosensitive polymer shell. First, it is observed that the relaxivities obtained are similar to the ones exhibited at the clinical field of 0.47 T (frequency of 20 MHz) and physiological temperature by commercial superparamagnetic MRI contrast agents such as Ferridex® (r_2=98 $s^{-1}mM_{Fe}^{-1}$ and r_1=24 $s^{-1}mM_{Fe}^{-1}$, r_2/r_1=4) or Resovist® (r_2=151 $s^{-1}mM_{Fe}^{-1}$ and r_1=25 $s^{-1}mM_{Fe}^{-1}$, r_2/r_1=6).[23] It is generally described in MRI textbooks that the r_2/r_1 ratio determines whether superparamagnetic NPs are best suited as positive contrast agents (with T_1-weighted imaging sequences) or negative contrast agents (with T_2-weighted imaging sequences). The solutions of the Bloch equations for the relaxation of the longitudinal (M_z) and transverse (M_{xy}) magnetization components to their equilibrium state indeed lead to a MRI signal that is proportional to the proton density of the solutions or tissues and to the product $\left(1 - e^{-TR/T_1}\right) \cdot e^{-TE/T_2}$, where TR is the repetition or read-out time of the sequence, and TE the inter-echo time. Thus, the sample signal becomes brighter than pure water when T_1 relaxation is accelerated while the T_2-effect is not already dominant (since the MRI signal is detected by an antenna in the transverse plane). Here, the uncoated magnetic NPs with a relatively low ratio r_2/r_1=3 can be used as positive (T_1-type) contrast agents, while the PDMAEMA-coated contrast agents present a T_2-type behaviour at low temperature (r_2/r_1=6 at 25°C) that decreases above the LCST (r_2/r_1=4 at 50°C).

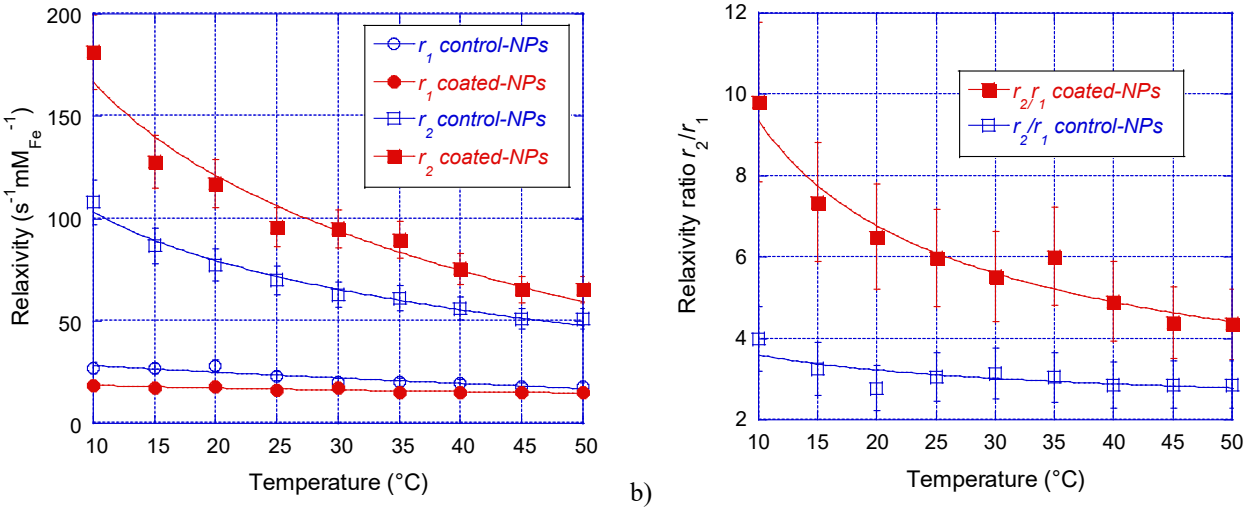

Figure 6: a) Longitudinal r_1 (circles) and transverse r_2 (squares) relaxivities of protons for uncoated S1S2 control-NPs (empty markers) and thermosensitive S1S2@AEAPTMS-AZ-PDMAEMA coated-NPs (filled markers); b) r_2/r_1 relaxivity ratios for S1S2 control-NPs (empty squares) and S1S2@AEAPTMS-AZ-PDMAEMA coated-NPs (filled squares). The solid lines are power law fits not based on a physical model.

It is noteworthy that the r_2/r_1 ratio remains relatively constant over the whole tested temperature range for the control uncoated NPs, as both r_1 and r_2 decrease with temperature, but their thermal behaviour is dictated solely by the variation of water diffusivity with temperature.[9] On the contrary, the r_2/r_1 ratio varies by a factor greater than 2 for the PDMAEMA-coated NPs, which proves that the temperature responsiveness of the shell is dominant. A similar two-fold decrease of the relaxometric ratio over an even more narrow temperature range (15°C) with liposomes encapsulating a paramagnetic compound was proposed by Terreno et al. to obtain an MRI response independent of concentration but dependant on pH or temperature.[24] In our case, the PDMAEMA shell is hydrated at low temperature and shrinks at higher temperature, particularly above the LCST. While the two samples are very different at 10°C (the coated and uncoated NPs behaving respectively as negative and positive contrast agents), they become more similar at 50°C. Several studies have proven that partial aggregation of superparamagnetic NPs is a means to increase their T_2-type behaviour. The fact that during the multiple steps of synthesis the colloidal stability of the NPs was disturbed could explain this difference. For the thermal behaviour, a simple explanation can be given in the context of the so called “outer

sphere" mechanism. For superparamagnetic MRI contrast agents, r_2 is determined by three parameters only:[25] the specific magnetization M_v, the internal magnetic volume fraction in the NP, and the "relaxometric size", defined as the minimum approach distance between water protons and the surface of the MNP. In the case of the magnetic core-shell PDMAEMA-coated NPs, these parameters are almost the same as for the uncoated particles when the polymer brush is swollen by water. However, when the polymer brush becomes dehydrated and collapses at the surface of the iron oxide core, it forms a layer impermeable to water molecules, which at the same time lowers the average magnetization of the particle (since the polymer layer is not magnetic) and increases the relaxometric size, thereby lowering the transverse relaxivity r_2 in a greater extent than r_1. To conclude, these iron oxide cores wrapped by a PDMAEMA shell that is highly hydrated below the LCST and impermeable to water molecules above it, and behave exactly like other thermosensitive MRI contrast agents recently described by Hannecart et al., with PDMAEMA instead of Jeffamine™ as a grafted thermosensitive brush.[9]

4.6 Detection of hydrodynamic size changes under magnetic field hyperthermia

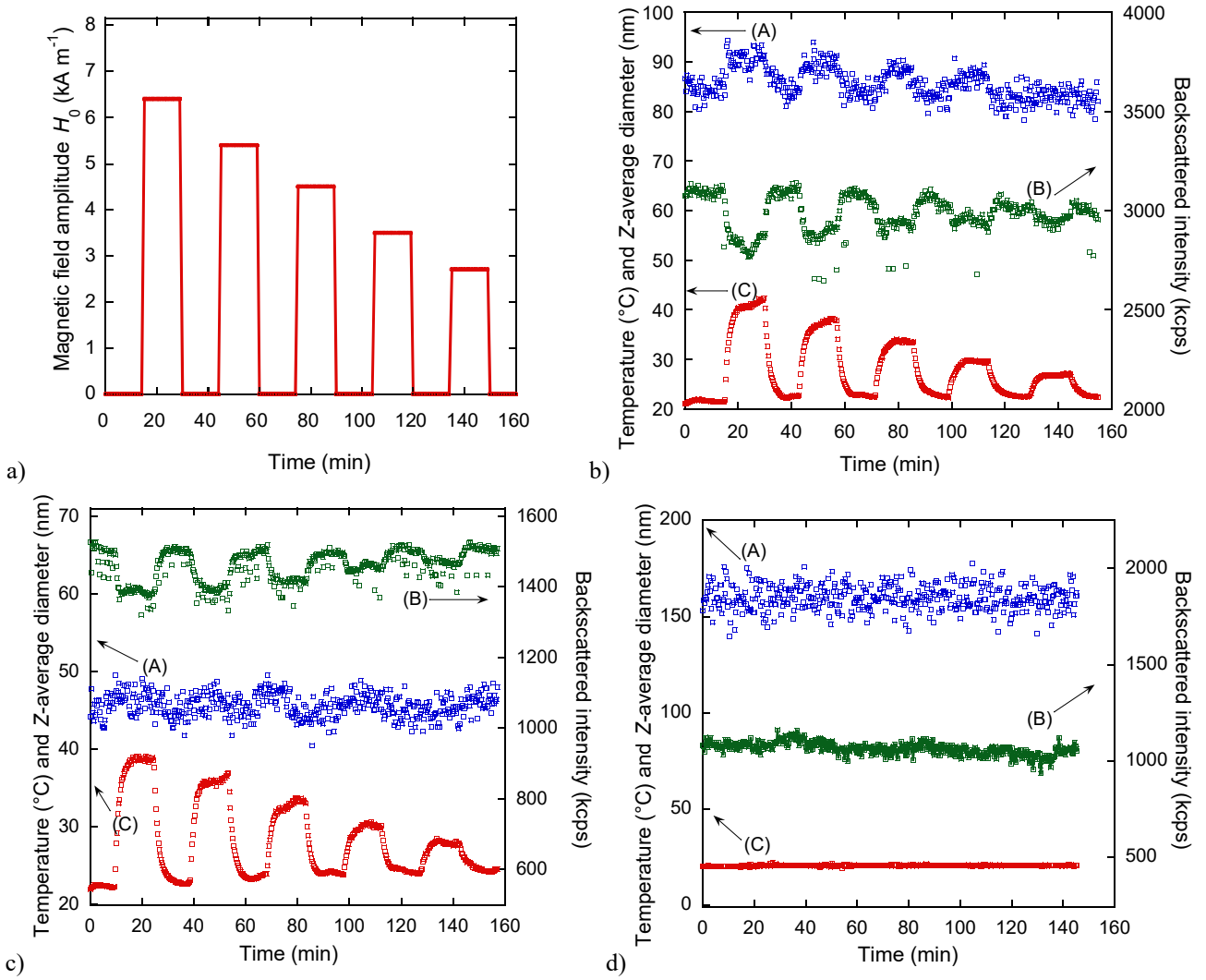

Figure 7: a) Magnetic field intensity *versus* time profile (at 755 kHz radiofrequency) applied to the sample and controls. *In situ* DLS/MH results (at ~1 g·L^{-1} iron oxide) obtained for: b) the C1C2@AEAPTMS-AZ-PDMAEMA coated sample, c) the uncoated non-thermosensitive C1C2@AEAPTMS control (both sample and control had a pH adjusted to 5.3-5.4), and d) polystyrene latexes as a non-magnetic non-thermosensitive control. The arrows indicate which axis to consider as ordinate for: (A) the Z-average hydrodynamic diameter as measured by 2nd order cumulant analysis; (B) the scattered light intensity on the photodetector (kcps) and (C) the temperature (°C) measured by the fibre optic probe *versus* time.

For these hyperthermia experiments, we chose the PDMAEMA-coated magnetic NPs of largest core size (C1C2). These also possess the largest specific heating properties, of approximately 50 $W \cdot g^{-1}$ under a RF magnetic field at f=785 kHz and of intensity H_0~6 $kA \cdot m^{-1}$.[26, 27] When a radiofrequency magnetic field is applied, heat is generated by the magnetic NPs, resulting in an increase in temperature first in their direct vicinity, and then following diffusion of heat into the bulk solution. With the PDMAEMA shell undergoing a transition from a hydrophilic to a hydrophobic state, the NPs exhibit transient variations of their hydrodynamic diameter directly correlated with the applied field intensity (Figure 7b). This thermal sensitivity is particularly high around 30°C, *i.e.* near the thermal transition of PDMAEMA. The system demonstrates a high level of reversibility; when the radiofrequency magnetic field is switched off, the hydrodynamic diameter returns back to its initial value around 82 nm. Concomitantly, a reversible variation of intensity is also observed, with a short characteristic time (~1.5 min). However, the backscattered intensity surprisingly decreases when the field is applied, which is contrary to what was expected from the off-line DLS curve *versus* temperature (Figure 5). Usually a destabilization of a colloidal dispersion induces large aggregates that scatter incoming laser light more intensely, because the scattered light intensity is proportional to the sixth-power of the diameter (in Rayleigh's approximation). Here the colloidal stability is ensured by electro-steric repulsion. Therefore the diameter increase (by 10 nm at most) can more likely be attributed to a decrease in the entropic component (present only when chains are swollen by water) and the NPs remain stable due to the electrostatic repulsion. The formed aggregates must also be very loose, otherwise the scattered intensity would increase. Interestingly, the backscattered intensity shows rapid variations with applied magnetic field intensity, meaning that the intensity curve (B) has a characteristic time of ~1.5 min comparable to the temperature curve (C) and is lower than the curve of diameter (A) showing few minutes of inertia.

Another way to represent the results of these experiments involves the elimination of the time variable and the plotting of diameter and intensity *versus* temperature measured by the fibre optic, for the PDMAEMA-coated (Figure 8a) and uncoated NPs (with only the positively charged aminosilane layer, Figure 8b). This shows that both the hydrodynamic diameter and the backscattered intensity were directly correlated to the *macroscopic temperature* for the thermosensitive NPs but only the intensity, not the diameter, for the control uncoated NPs.

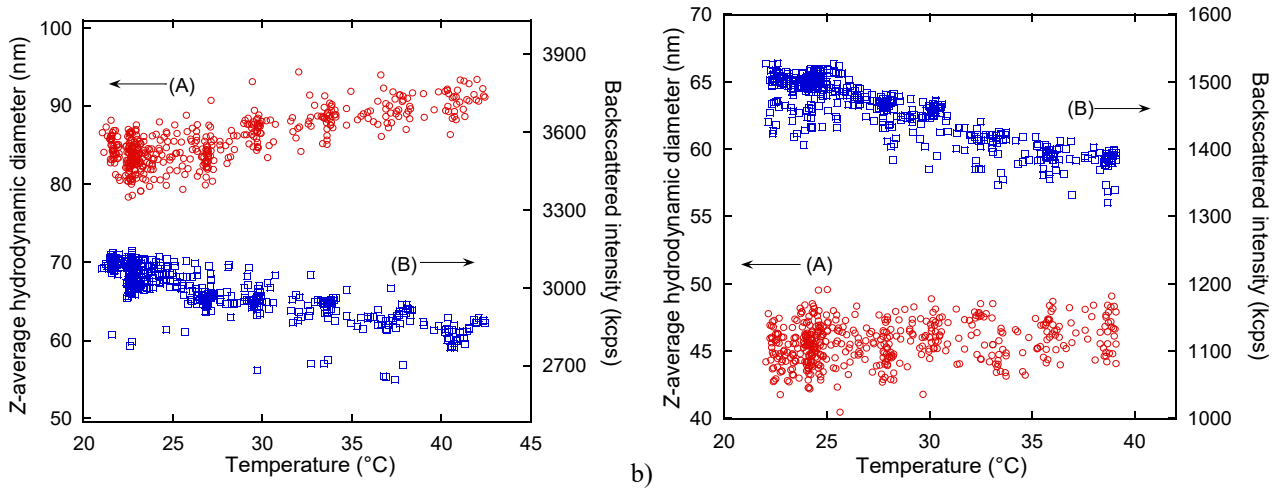

Figure 8: Hydrodynamic diameter (A) and backscattered intensity (B) plotted *versus* temperature for the thermosensitive sample C1C2@AEAPTMS-AZ-PDMAEMA and the C1C2@AEAPTMS control, under an alternating magnetic field of intensity H_0=6.4 $kA \cdot m^{-1}$ and frequency f=755 kHz. Iron oxide concentrations were ~1 $g \cdot L^{-1}$ and pH adjusted to 5.3-5.4.

4.7 Control experiments

In order to fully demonstrate that NPs with a magnetic core and a thermosensitive polymer corona are required in order to obtain a variation of hydrodynamic size under a RF magnetic field, complementary

experiments of *in situ* DLS under an applied RF magnetic field were carried on with non-thermosensitive and non-magnetic polystyrene latexes. For these particles, no increase of temperature was observed under an applied RF magnetic field, suggesting that no parasitic heating ascribed to Joule or eddy current effects occurred in the experimental system in the absence of magnetic NPs. Apart from experimental noise, the recorded diameters and intensities were also constant over time for the application of different magnetic field intensities (Figure 7d).

The comparison of the results of *in situ* DLS under RF magnetic field of C1C2@AEAPTMS-AZ-PDMAEMA magnetic and thermosensitive NPs (Figure 7b), of C1C2@AEAPTMS, magnetic but not thermosensitive NPs (Figure 7c), and of non-magnetic and non-thermosensitive polystyrene latexes (Figure 7d) highlights that the variations of hydrodynamic diameters observed in the first case are specific to the thermosensitivity of the polymer shell and to the magnetic field-induced hyperthermia. Regarding the variations of backscattered intensity observed for magnetic NPs (without polymer) but not for non-magnetic latexes, this phenomenon could be ascribed to the magnetic dichroism (also called "Faraday rotation") inherent of magnetic NPs. Due to a direct coupling between the magnetic moments of the NPs aligned by the magnetic field and their optical anisotropy axis when a longitudinal magnetic field is applied (*i.e.* oriented parallel to the incident beam), the polarisation of light rotates by an angle θ_F as measured in transmission through the sample or in reflection. This angle proportional to the field intensity can be as high as $15°\cdot cm^{-1}$ at 633 nm at high magnetic field (saturated moments) and changes in sign with the field direction.[28] Although we cannot exclude such direct influence of the magnetic field on the optical detection during *in situ* DLS measurement under RF magnetic field, we did not observe a variation of the backscattered intensity on any of the NPs used under a static magnetic field. This last control experiment was performed by inserting the sample holder of the remote head of the Cordouan VASCO Flex™ setup inside a 1000-turn coil producing a static magnetic field in the same direction as in the RF magnetic hyperthermia experiment, and with the same series of field intensities as for the magnetic hyperthermia experiments (Figure S4).

5. Conclusion

In this article, we described the synthesis of magnetic NPs comprising an iron oxide core and thermosensitive polymer shell exhibiting reversible size variation when subjected either to macroscopic heating or magnetic heating induced by a radiofrequency magnetic field. These PDMAEMA-coated magnetic NPs can be used as MRI contrast agents, with a transition from a purely negative (T_2-type) contrast at low temperature to a less efficient T_2-type contrast at high temperature but also potentially positive (T_1-type), due to a lower r_2/r_1 relaxivity ratio. We designed an experiment that enabled *in situ* DLS under RF magnetic heating by placing a fibre-based backscattering remote-head DLS as close as possible to the inductor coil of the MH generator. The hydrodynamic diameters and the backscattered intensity of coated magnetic NPs and of uncoated (control) NPs were monitored on-line during the treatment with the RF magnetic field. It was found that the hydrodynamic diameter and the backscattered intensity correlated well with the macroscopic temperature changes measured independently by standard fibre optic thermometry. These results are promising as they showed for the first time that the size variation of NPs can be measured without switching off the magnetic field, which is important as the swelling/collapsing response time of a polymer brush has very fast kinetics. In future work, the RF magnetic field application will be extended to higher powers *via* the replacement of metallic parts in the remote head of the DLS setup. This may enable further insights into the mechanisms of heat generation and dissipation by magnetic NPs at the scale of the polymer shell, less than 10 nm. The temperature profile in the close vicinity of NPs is an intensively debated question in view of the standardization and optimisation of medical magnetic hyperthermia and magnetic-field triggered drug delivery. Right now the probed temperature is the macroscopic solvent temperature. However in near future, a gain in sensitivity and speed of this method might achieve to evidence the temperature gap between the NP

surface and the solvent that was suspected in several other studies of literature. In addition, the same *in situ* DLS methodology can be applied to study other kinds of thermogenic NPs such as plasmonic NPs under visible or near-infrared illumination.

Acknowledgements

The Department of Science & Technology of the University of Bordeaux (APUB1- ST2014) and the Agence Nationale de la Rercherche (ANR-13-BS08-0017) are acknowledged for financial support. The Natural Sciences and Engineering Research Council of Canada is thanked for a CGS scholarship (ADW) and Discovery Grant (ERG). The authors are also indebted to Dr Eneko Garaio from UPV-EHU in Bilbao for his useful advice on the electronic interfacing of the fibre optic thermometer and on the measurement of magnetic field intensity. Transmission electron microscopy images were taken at the Bordeaux Imaging Center (BIC) of the University of Bordeaux with the acknowledged help of Sabrina Lacomme and Etienne Gontier.

References

1. Q. A. Pankhurst, N. T. K. Thanh, S. K. Jones and J. Dobson, Journal of Physics D: Applied Physics **42** (22), 224001 (2009).
2. J. Thevenot, H. Oliveira, O. Sandre and S. Lecommandoux, Chemical Society Reviews **42** (17), 7099-7116 (2013).
3. A. Riedinger, P. Guardia, A. Curcio, M. A. Garcia, R. Cingolani, L. Manna and T. Pellegrino, Nano Letters **13** (6), 2399-2406 (2013).
4. T. T. T. N'Guyen, H. T. T. Duong, J. Basuki, V. Montembault, S. Pascual, C. Guibert, J. Fresnais, C. Boyer, M. R. Whittaker, T. P. Davis and L. Fontaine, Angewandte Chemie International Edition **52** (52), 14152-14156 (2013).
5. J. T. Dias, M. Moros, P. del Pino, S. Rivera, V. Grazú and J. M. de la Fuente, Angewandte Chemie International Edition **52** (44), 11526-11529 (2013).
6. M. Moros, A. Ambrosone, G. Stepien, F. Fabozzi, V. Marchesano, A. Castaldi, A. Tino, J. M. de la Fuente and C. Tortiglione, Nanomedicine, 1-17 (2015).
7. A. Meffre, B. Mehdaoui, V. Connord, J. Carrey, P. F. Fazzini, S. Lachaize, M. Respaud and B. Chaudret, Nano Letters **15** (5), 3241-3248 (2015).
8. J. Soussi, S. Volz, B. Palpant and Y. Chalopin, Applied Physics Letters **106** (9), 093113 (2015).
9. A. Hannecart, D. Stanicki, L. Vander Elst, R. N. Muller, S. Lecommandoux, J. Thevenot, C. Bonduelle, A. Trotier, P. Massot, S. Miraux, O. Sandre and S. Laurent, Nanoscale **7** (8), 3754-3767 (2015).
10. S. Karamdoust, B. Yu, C. V. Bonduelle, Y. Liu, G. Davidson, G. Stojcevic, J. Yang, W. M. Lau and E. R. Gillies, Journal of Materials Chemistry **22** (11), 4881-4889 (2012).
11. G. J. P. Britovsek, J. England and A. J. P. White, Inorganic Chemistry **44** (22), 8125-8134 (2005).
12. W. T. Eckenhoff, S. T. Garrity and T. Pintauer, European Journal of Inorganic Chemistry **2008** (4), 563-571 (2008).
13. W. Jakubowski and K. Matyjaszewski, Macromolecules **38** (10), 4139-4146 (2005).
14. R. Massart, IEEE Transactions on Magnetics **17** (2), 1247-1248 (1981).
15. P. Arosio, J. Thévenot, T. Orlando, F. Orsini, M. Corti, M. Mariani, L. Bordonali, C. Innocenti, C. Sangregorio, H. Oliveira, S. Lecommandoux, A. Lascialfari and O. Sandre, Journal of Materials Chemistry B **1** (39), 5317-5328 (2013).
16. E. Duguet, S. Mornet and J. Portier, PCT/FR 2004/001169 WO 2004107368 A3 (2004).
17. R. Srinivasan, L. P. Tan, H. Wu, P.-Y. Yang, K. A. Kalesh and S. Q. Yao, Organic & Biomolecular Chemistry **7** (9), 1821-1828 (2009).
18. M. A. Anisimov, I. K. Yudin, V. Nikitin, G. Nikolaenko, A. Chernoutsan, H. Toulhoat, D. Frot and Y. Briolant, The Journal of Physical Chemistry **99** (23), 9576-9580 (1995).
19. D. L. Conover, W. E. Murray, J. M. Lary and P. H. Johnson, Bioelectromagnetics **7** (1), 83-90 (1986).
20. C. Henoumont, S. Laurent and L. Vander Elst, Contrast Media & Molecular Imaging **4** (6), 312-321 (2009).

21. W. Agut, A. Brûlet, C. Schatz, D. Taton and S. Lecommandoux, Langmuir **26** (13), 10546-10554 (2010).
22. F. A. Plamper, M. Ruppel, A. Schmalz, O. Borisov, M. Ballauff and A. H. E. Müller, Macromolecules **40** (23), 8361-8366 (2007).
23. Y.-X. J. Wang, Quantitative Imaging in Medicine and Surgery **1** (1), 35-40 (2011).
24. E. Terreno, D. Delli Castelli, C. Cabella, W. Dastrù, A. Sanino, J. Stancanello, L. Tei and S. Aime, Chemistry & Biodiversity **5** (10), 1901-1912 (2008).
25. Q. L. Vuong, J.-F. Berret, J. Fresnais, Y. Gossuin and O. Sandre, Advanced Healthcare Materials **1** (4), 502-512 (2012).
26. E. Garaio, J. M. Collantes, J. A. Garcia, F. Plazaola, S. Mornet, F. Couillaud and O. Sandre, Journal of Magnetism and Magnetic Materials **368**, 432-437 (2014).
27. E. Garaio, O. Sandre, J.-M. Collantes, J. A. Garcia, S. Mornet and F. Plazaola, Nanotechnology **26** (1), 015704 (2015).
28. F. Choueikani, F. Royer, S. Douadi, A. Skora, D. Jamon, D. Blanc and A. Siblini, Eur. Phys. J. Appl. Phys. **47** (3), 30401 (2009).

Supporting information:

Thermosensitive polymer-grafted iron oxide nanoparticles studied by *in situ* dynamic light backscattering under magnetic hyperthermia

Gauvin Hemery[1], Elisabeth Garanger[1], Sébastien Lecommandoux[1], Andrew D. Wong[2], Elizabeth R. Gillies[2], Boris Pedrono[3], Thomas Bayle[3], David Jacob[3], and Olivier Sandre[1*]

1. Synthesis and characterization of the propargyl-terminated PDMAEMA chains

(A)

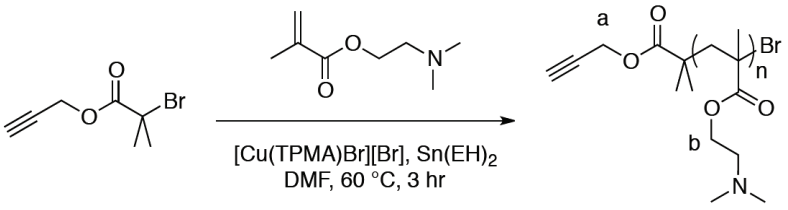

(B)

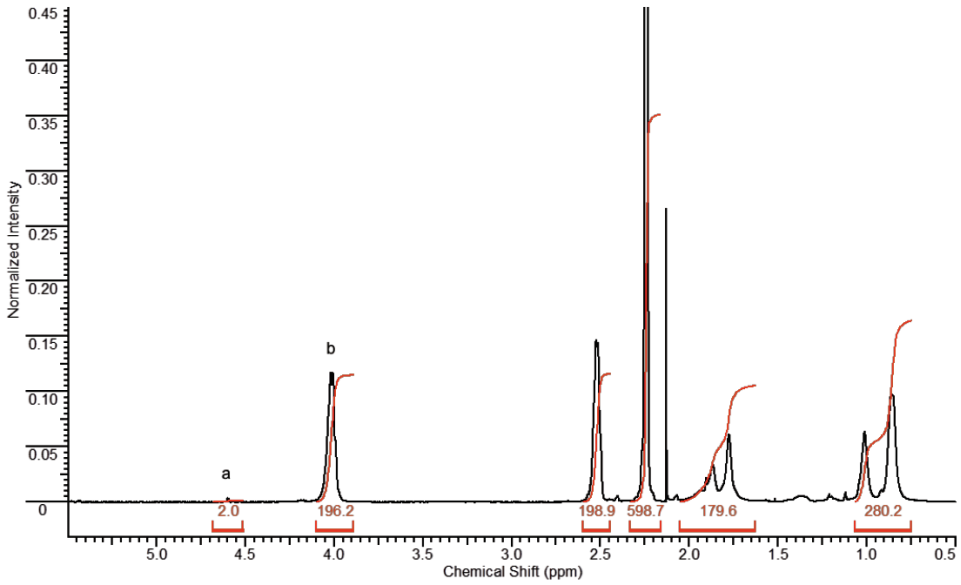

(C)

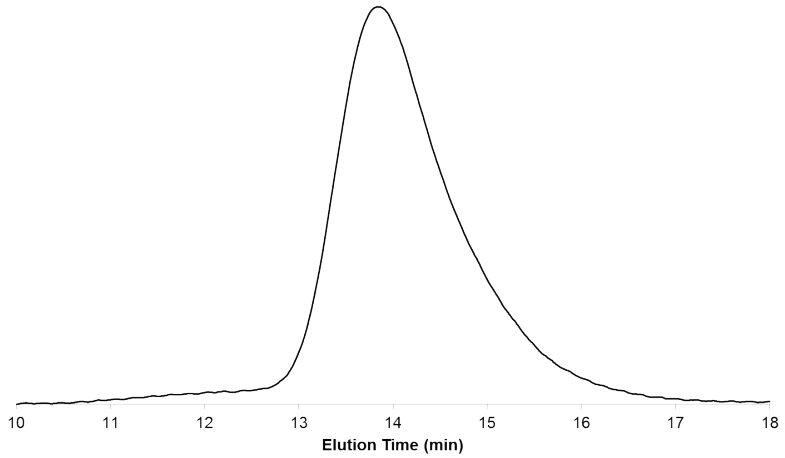

Figure S1. (A) Scheme for the synthesis of PDMAEMA by ARGET ATRP. Labels a and b correspond to the resonances in ^{1}H-NMR (B) used to determine the degree of polymerization (DP=98) and number-average molar mass (M_n^{NMR}=15.4 kDa). (C) Size-exclusion chromatography (SEC) traces of PDMAEMA, calibrated with poly(methyl methacrylate) (PMMA) standards leading to the mass dispersity index $Đ=M_w/M_n$=1.29 and M_n^{SEC}=9.85 kDa.

2. Synthesis of the MNPs

Superparamagnetic NPs made of maghemite (γFe_2O_3) were synthesized in water according to Massart's procedure. The reactants were prepared by introducing 180 g of $FeCl_2{\cdot}4H_2O$ (0.9 mol), 100 mL of HCl 37% and 500 mL of distilled water in a 1 L beaker. A magnetic stir bar was used to assist in the dissolution of $FeCl_2{\cdot}4H_2O$. 715 mL of $FeCl_3{\cdot}6H_2O$ solution (1.5 mol) were poured into a 5 L beaker, later used for the reaction. After the complete dissolution of $FeCl_2$, the solution obtained was poured onto the 5 L beaker, the resulting solution was filled to 3 L with distilled water. A mechanical agitator was used at 800 rounds per minute (rpm). One litre of a concentrated ammonia 30% solution (7 mol) was then added promptly into the acidic iron salts mixture. This alkaline co-precipitation of the ferrous and ferric salts almost instantaneously produced a black solid suspension of magnetite (Fe_3O_4) nanocrystals also called ferrous ferrite ($FeO{\cdot}Fe_2O_3$). After 30 minutes of stirring at 800 rpm, the Fe_3O_4 NPs were attracted by a strong ferrite magnet (152×101×25.4 mm^3, Calamit Magneti™, Milano-Barcelona-Paris). Then, the supernatant (2.25 L) containing non-magnetic ferrihydrites (reddish flakes) was aspirated with a water pump vacuum and discarded. The black magnetic precipitate was washed with 1 L of water, stirring for 10 min. Next, the beaker was placed over the strong magnet for magnetic sedimentation. The clear supernatant was removed by using water pump vacuum. After sedimentation on the ferrite magnet, the flocculate was acidified with 0.26 L of nitric acid (69%), completed up to 2 L with water, and stirred 30 min. The acidification and separation steps were repeated. In order to completely oxidize magnetite into maghemite, the solid phase was separated from the supernatant (1.5 L, red) and immersed in a boiling solution of ferrite nitrate (0.8 mol). After 30 min of stirring at 90-100°C, the suspension changed to the red colour characteristic of maghemite γFe_2O_3. Finally, free ions in excess were removed by washing with water, acetone and diethyl-ether. This stable ferrofluid was stirred for 10 min, after which 360 mL of concentrated nitric acid were added to destabilize the suspension. Having introduced 1 L of acetone and stirring the ferrofluid for 10 min, the steps of sedimentation and suction were repeated in order to remove the ions in excess. 500 mL of diethyl-ether was added and the suspension was stirred for 10 min to remove the traces of acetone. The steps of sedimentation and suction were repeated. In the end, the NPs readily dispersed in water to form a true "ionic-ferrofluid" made of maghemite NPs. The iron-oxide surface bears positive charges due to adsorption of protons in acidic media, in that case a dilute HNO_3 solution at pH between 1.2 and 1.7. This ferrofluid remains in a monophasic state under the application of a magnetite field of arbitrary value.

3. Size-sorting process: magnetic sedimentation

Size-sorting by magnetic sedimentation was the first post-synthesis process to be applied. When stable in acidic water, their dipolar attractions (van der Waals and magnetic) are counterbalanced by electrostatic (double-layer) repulsion arising from the cationic charges at their surfaces. The addition of an excess of HNO_3 (pH~0.7-0.8) causes the screening of the charges. The fluid was then allowed to sediment on a permanent magnet. Two phases were obtained in an intermediate state of destabilization. The bottom phase is named the "concentrated phase" (referred as C), containing larger particles on average. The phase at the top is named the supernatant (referred as S); it is more dilute and contains smaller particles. The two phases were separated macroscopically, and the concentrated phase was re-dispersed by the addition of water. This size-sorting method was repeated two times, leading to four fractions, namely S1S2, S1C2, C1S2, and C1C2.

4. Grafting of the aminosilane on the surface of the MNPs

A 3-neck boiling flask was half immersed in a bath at a set temperature of 50°C. A water condenser was assembled on the boiling flask and a rod stirrer was inserted through the glassware, its rod passing through the inside of the condenser, its helix immerged in the boiling flask, and the other end being inserted in the socket of a mechanical agitator. 90 mL of ethanol were added in the boiling flask, along with 5 mL of water and 5 mL of the S1S2 suspension at an equivalent iron concentration of 1.93 $mol \cdot L^{-1}$. 530 µL of AEPTMS were added drop by drop, the pH of the solution being simultaneously adjusted with dilute nitric acid to a value of 2 in order to assist in the dispersion of the NPs and the hydrolysis of the methoxysilane. After 1 hour the pH was gradually increased to 7 and the temperature set at 90°C for 1 hour, allowing the condensation of the aminosilane on the surface of the NPs. After completion of the reaction the ferrofluid was transferred to a 400 mL beaker and allowed to sediment over a strong permanent magnet. The supernatant was removed using a vacuum flask linked to a membrane pump and the pellet was washed two times with 100 mL of methanol. After this precipitation-redispersion process, 50 mL of water with its pH adjusted to 3 with dilute HNO_3 was poured on the pellet, and the colour of the fluid turned deep black.

5. Characterization of the cross-liking agent by NMR spectroscopy

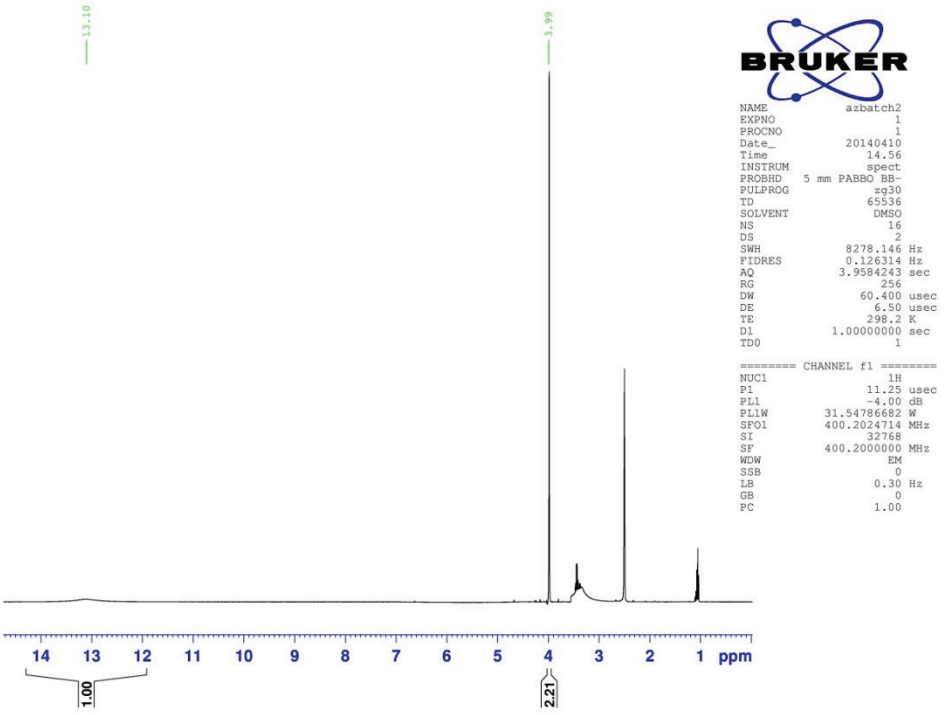

Figure S2. ^{1}H NMR spectrum of the synthesized azidoacetic acid (AZ).

6. Characterization of the polymer-grafted MNPs by TGA

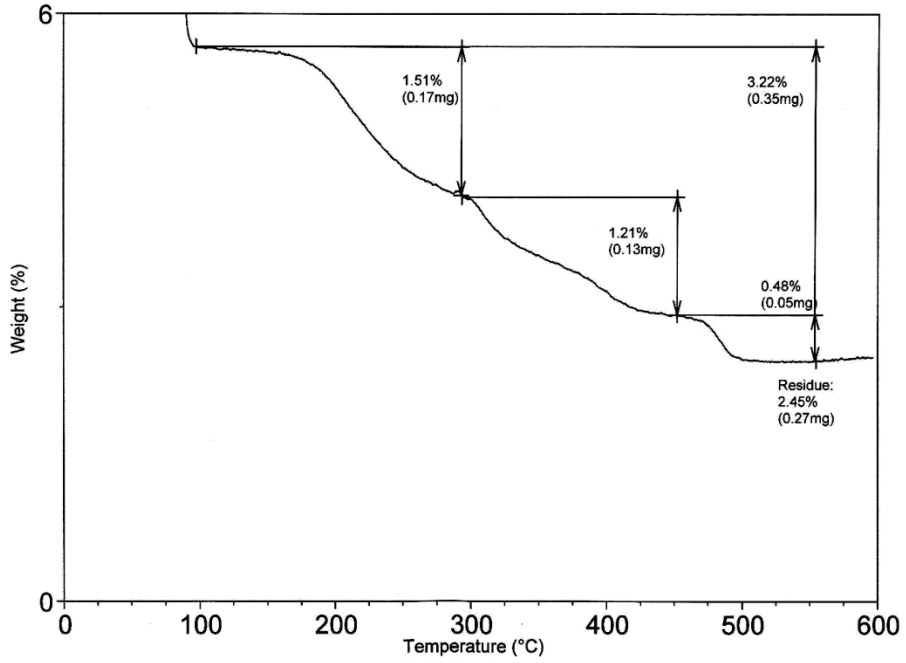

Figure S3. Thermogravimetric analysis (TGA) of S1S2@AEAPTMS-AZ-PDMAEMA coated-NPs

The mass of organic material composes 54% of the overall mass. The reacted aminosilane represents 7% of the mass. Assuming a NP of 10 nm of diameter, and knowing the molecular weight of the reacted aminosilane, the density of the core (~5 $g \cdot cm^{-3}$) and relative mass fraction of aminosilane and core, the density grafting of molecule per nm^2 can be determined. In this case it represents a density grafting of 6.7 molecules per nm^2. This value is high but not improbable, and indicates a thick corona of silane on the surface. During the coating process the alkoxysilane is hydrolysed at low pH, resulting in the formation of silanol by the loss of the methoxy groups into methanol. In order to favour the condensation of the silanols on the surface of the NPs rather than the self-polymerization, the pH was quickly increased to a basic value and water was present in a low amount. This organic shell was possibly deposited as multilayers, interconnected through a loose network structure, or intermixed, or both, but in any form it represents a substrate for the attachment of the polymer brushes; it provides amine groups which allow the grafting of azidoacetic acid. The primary amines may not be all functionalizable as from a diffusion point of view, the amide bond formation reaction takes place with water as a solvent, acid medium as catalyst, and the azidoacetic acid molecules need to access the primary amines at the NP surface. This explains why based on TGA only ~6.1% of the amines underwent a reaction. The remaining amines participate in the colloidal stability of the NPs by retaining a positive charge. PDMAEMA was then grafted quantitatively, which is characteristic of copper assisted azide-alkyne cycloaddition reactions, which generally occur in high yields.

	M **(g·mol^{-1})**	***m*** **(g)**	***n*** **(mmol)**	**Conversion (%)**
Aminosilane	118	7.01	59.4	6.1
Azidoacetic acid	100	0.36	3.6	
PDMAEMA	13000	46	3.5	98.3

7. Control of the in situ DLS under a constant (DC) magnetic field

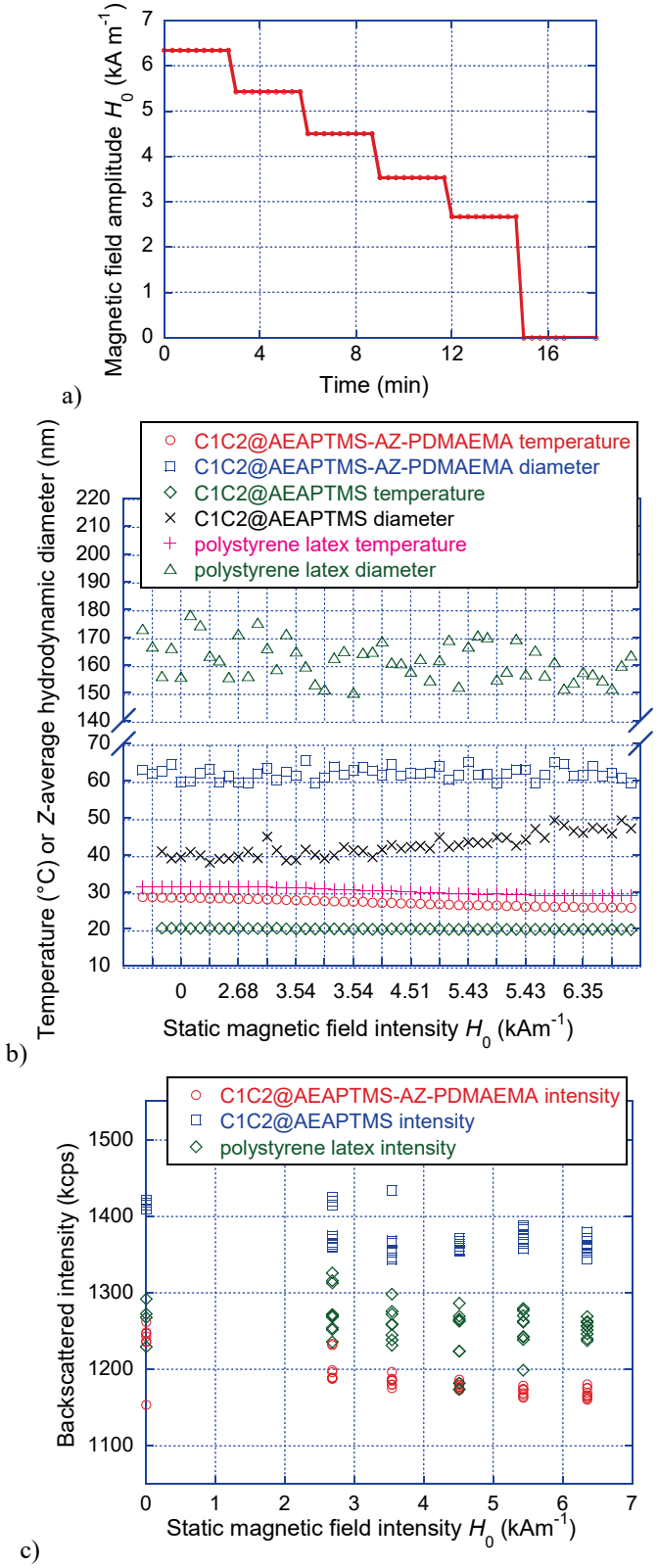

Figure S4: *In situ* DLS experiment under static (DC) magnetic field. The sample holder was placed inside a solenoid producing a magnetic field parallel to the incident laser beam direction. a) Magnetic field intensity profile along time; b) Temperature and diameter plotted *versus* applied magnetic field; c) Backscattered intensity *versus* applied magnetic field. These variations are not significant, therefore one can conclude that a DC magnetic field has not effect on these systems.